Deformation twinning in the full-α martensitic Ti–25Ta–20Nb shape memory alloy

Emmanuel Bertrand, Philippe Castany, Yang Yang, Edern Menou, Thierry Gloriant

Deformation twinning in the full-α'' martensitic Ti-25Ta-20Nb shape memory alloy

Emmanuel Bertrand[1,*], Philippe Castany[2], Yang Yang[2], Edern Menou[1], Thierry Gloriant[2]

[1] *Institut des Matériaux Jean Rouxel (IMN), Université de Nantes, CNRS, Rue Christian Pauc, BP 50609, 44306 Nantes Cedex 3, France*

[2] *INSA Rennes, Institut des Sciences Chimiques de Rennes (ISCR CNRS 6226), 20 avenue des Buttes de Coësmes, F-35708 Rennes Cedex 7, France*

** Corresponding author: emmanuel.bertrand@univ-nantes.fr*

Tel.: +33 2 40 68 31 28, Fax: +33 2 40 68 31 99

Abstract

Deformation twinning of the Ti-25Ta-20Nb (mass%) shape memory alloy is characterized using EBSD and TEM. The selfaccommodating α'' microstructure is shown to be first deformed using $\{111\}_{\alpha''}$ type I and $<211>_{\alpha''}$ type II reorientation twinning. Plastic deformation occurs further by plastic twinning with a new $\{130\}<310>_{\alpha''}$ twinning system. Maximum lattice deformation calculation is a relevant parameter to predict the variant of martensite that is favored during the reorientation process. Conversely, Schmid factor analysis can be used to predict the selection of $\{130\}<310>_{\alpha''}$ twinning variants during deformation. Analogy between $\{130\}<310>_{\alpha''}$ and $\{332\}<113>_{\beta}$ twinning systems is highlighted.

Keywords: EBSD; Twinning; α'' martensite; Titanium; Shape memory alloy

1 Introduction

Metastable β titanium alloys are a wide field of interest since the last decades due to the possibility to obtain Ni-free superelastic alloys using fully biocompatible elements only [1-10]. In these alloys, the amount of β-stabilizing elements (such as Nb, Ta, Mo…) is sufficient to retain metastable β phase at room temperature by quenching from the high temperature β domain. Then, superelasticity is generally obtained by a stress-induced martensitic transformation from the β phase into the C-centered orthorhombic α'' martensite. From the fundamental point of view, deformation of these alloys involves numerous mechanisms such as stress-induced martensitic transformation [2,4,11-16], twinning [5,17-20] and dislocation slip [21-24] that have been widely studied.

With a slightly lower content of β-stabilizing elements, the β phase is directly decomposed into α'' martensite during the quench. Each β grain transforms thus in martensite with 6 equiprobable lattice correspondence variants (CVs) given in Table 1, each variant of martensite being in Orientation Relationship (OR) with the parent β phase according to: $\{-110\}_{\beta}$ // $(001)_{\alpha''}$ and $<111>_{\beta}$ // $[110]_{\alpha''}$ [25]. In such alloys, the transformation of β phase into α'' martensite leads to a selfaccommodating microstructure: the shears induced by the transformation of each variant of martensite annihilate themselves so as to minimize the change in shape of the ex-β grain during the transformation [26]. As a consequence, in a given ex-β grain, variants of α'' martensite are auto-organized by groups in twinning relationship and share either a $\{111\}_{\alpha''}$ plane (type I twinning) or a $<211>_{\alpha''}$ direction (type II twinning) [27-29].

Table 1. Lattice correspondence variants (CV) derived from the β/α'' orientation relationship [28].

Variant			
CV1			
CV2			
CV3			
CV4			
CV5			
CV6			

Due to the selfaccommodating microstructure, full α'' alloys may exhibit shape memory effect. Indeed, when a stress is applied, the first activated deformation mechanism is the growth of variants which are favorably oriented to the detriment of others: the selfaccommodating microstructure is thus reoriented by the stress [30]. This mechanism is highlighted by a stress plateau on stress-strain curves and, ideally, each ex-β grain is transforming in one unique α'' variant during this process. This phenomenon is not reversible at constant temperature, leading to remaining deformation after a release of the stress. Shape memory effect is thus obtained by heating the reoriented microstructure above a temperature named A_f (austenite finish) in shape memory alloys: the α'' martensite transforms back to β phase in the original orientation because of the lattice correspondence, which restores the original shape of each grain. It can be also noticed that, if the material is deformed more than the strain corresponding to the stress plateau, irreversible mechanisms can take place, leading to permanent strain after heating above A_f.

Literature shows that deformation mechanisms of metastable β titanium alloys are widely studied as well as the microstructure of unstrained α'' shape memory alloys. However, to the authors' knowledge, there is almost no study about mechanisms of plastic deformation in α'' shape memory alloys. The $\{111\}_{\alpha''}$ type I and $<211>_{\alpha''}$ type II twinning systems were deeply investigated [27-29], but these twinning are involved during reorientation of

selfaccommodating microstructure and are not strictly mechanisms of plastic deformation. Finally, $\{110\}_{\alpha''}$ compound twinning was reported in a deformed α" microstructure, but in a specific case where twins was observed only at the surface of tensile specimen [31]. No other study about deformation twinning in bulk α" martensite were found elsewhere. However, plastic deformation and especially deformation twinning may have a detrimental influence on the shape recovery of martensitic shape memory alloys. Indeed, the magnitude of the recoverable strain obtained from reorientation processes is reduced when such microstructures are plastically twinned. Consequently, the knowledge of possible twinning modes is of key interest in order to try to impede their occurrence and thus improve the shape recovery of α" titanium-based shape memory alloys. Then, this paper focuses on twinning occurring during the deformation of a full α'' titanium shape memory alloy. A special attention is brought to the characterization of twins involved in plastic deformation and the comparison with twinning systems observed in metastable β titanium alloys.

2 Materials and methods

The Ti-25Ta-20Nb (mass%) alloy was elaborated by Cold Cruicible Levitation Melting (CCLM). This technique ensures melting of alloys with a high content of tantalum which has a higher melting point than titanium. The elements used are commercially pure titanium and pure niobium and tantalum. The ingots underwent a thermomechanical protocol composed of a solution treatment at 950°C for 20 h, cold rolling (CR=98%) and finally a recrystallization treatment at 850°C for 0.5 h before quenching in water.

The phases repartition is determined by X-ray diffraction (XRD) using a Bruker D8 Advance diffractometer with LynxEye detector and Cu Kα radiation.

Tensile tests are carried out at room temperature at a strain rate of 10^{-4} s^{-1} using an Instron E3000 tensile machine on normalized flat tensile specimens strained along the rolling

direction. Tensile specimens after interrupted tensile tests are used for the characterization of twins. Shape memory effect is also characterized by an interrupted tensile test followed by heating until 250 °C with a heating rate of 5°C/min in order to measure the shape recovery and the characteristic temperatures of the α" to β phase transformation. As the tensile machine used is equipped with a furnace, heating is performed immediately after the tensile test in the same machine.

Electron BackScattered Diffraction (EBSD) studies are carried out in a Merlin scanning electron microscope (SEM) from Carl Zeiss equipped with a Nordlys 2 camera on tensile specimens strained until 6%. An accelerating voltage of 20 kV and a probe current of 10 nA are used. The samples are prepared by mechanical polishing to a "mirror finished" state. Chemical etching with a solution of 5% HF, 5% HNO_3 and 90% H_2O (vol.%) is used to remove the residual deformation layer induced by polishing.

Transmission Electron Microscopy (TEM) observations are performed using a Jeol 2100 machine operating at 200 kV. Thin foils were cut from tensile specimens, mechanically polished with SiC papers and finally thinned using a twin-jet electropolishing system with a solution of 4 % perchloric acid and 96 % methanol (vol.%) at -25°C.

3 Structural and mechanical characterization

Fig. 1 shows optical micrograph of the Ti-25Ta-20Nb alloy and associated X-rays diffractogram. The microstructure is composed of "grains" in which thinner microstructure composed of needles is visible. The X-rays diffractogram is fully indexed by α'' phase and no trace of β phase is detected. Its lattice parameters which are strongly dependent on the chemical composition [11] are measured as a=0.3174 nm, b=0.4826 nm and c=0.4638 nm. As a summary, and as previously shown [32], the microstructure is composed of ex-β grains which were decomposed during the quench into a selfaccommodation α'' martensitic

microstructure, following the classical OR between α'' martensite and β phase. At a finer scale, the presence of thin martensite plates is confirmed by TEM observations (Fig. 2). Depending on ex-β grain, typical V-shaped morphology of martensite can be observed (Fig. 2a) or a more complex arrangement of plates (Fig. 2b) due to different viewing orientation of each grain regarding the plane of the micrograph [28].

Fig. 3 (a) shows the tensile curve until rupture. One can notice the high ductility of this alloy (above 30%) and the presence of a "stress plateau" between 1 and 3% which corresponds to the reorientation of the martensite. This plateau is then followed by a slight increase of the stress between 3% and 30% and reached the maximum resistance of 550 MPa. The Young's modulus is measured as 87 GPa. The expected shape memory effect of this alloy is characterized from an interrupted tensile test until 3% strain followed by heating as presented on Fig. 3 (b): after the interrupted tensile test, most of the deformation is not reversible but is totally recovered after heating proving the shape memory effect. The austenite start temperature (A_s) is measured as 205 °C and the austenite finish temperature (A_f) as 232 °C from intersection of tangents.

4. Identification of twining systems

4.1. EBSD analysis

Fig. 4 shows EBSD maps of a tensile specimen strained until 6%. The present study will focus on one single ex-β grain gathering all the phenomena which are observed in the rest of the tensile specimen. One can see on the band contrast map (Fig. 4a) that several bands of deformation are present: Large bands cross the whole ex-β grain and smaller ones are limited to a reduced part of the ex-β grain. The obtained EBSD data are perfectly indexed by α'' phase as illustrated on the EBSD map in Euler angles on Fig. 4b. This map shows that 4 crystallographic orientations (named $O1_{\alpha''}$ to $O4_{\alpha''}$, respectively) can be determined in this

ex-β grain. The left part of the ex-β grain is occupied by $O1_{\alpha''}$ only, which means that a single α" variant remains instead of the 6 initially present and thus that this part of the grain has been fully reoriented. Additionally, the large deformation bands crossing the whole ex-β grain correspond to $O3_{\alpha''}$ and $O4_{\alpha''}$, while the smaller deformation bands are composed $O2_{\alpha''}$ domains surrounded by $O1_{\alpha''}$.

In order to determine the orientation relationships between each domain, and thus determine the twinning systems that potentially occurred during deformation, stereographic projections are drawn from EBSD data for the 4 crystallographic orientations observed on Fig. 4b. On each stereographic projection (Fig. 5), only some poles and traces of interest are represented to ensure a better readability. Let us consider first the orientation relationship between $O1_{\alpha''}$ and $O2_{\alpha''}$, that correspond to the thinner deformation bands on Fig. 4b. Both $O1_{\alpha''}$ and $O2_{\alpha''}$ share a common $\{111\}_{\alpha''}$ pole: $)_{\alpha''}$ for $O1_{\alpha''}$ (Fig. 5a) and $(111)_{\alpha''}$ for $O2_{\alpha''}$ (Fig. 5b). A rotation of 180° around this common pole of $O2_{\alpha''}$ leads to $O1_{\alpha''}$. Thus, $O1_{\alpha''}$ and $O2_{\alpha''}$ are in twinning relationship with the $\{111\}_{\alpha''}$ type I twinning system which was already observed in selfaccomodating microstructures [28,29].

Concerning the orientation relationship between $O1_{\alpha''}$ and $O3_{\alpha''}$ which corresponds to a large deformation band in Fig. 4, a careful examination of stereographic projections shows that both orientations have a common $\{130\}_{\alpha''}$ pole and a common $<310>_{\alpha''}$ direction (Fig. 5a and 5c). A rotation of 180° around the $(1\bar{3}0)_{\alpha''}$ pole or $[310]_{\alpha''}$ direction of $O1_{\alpha''}$ transforms $O1_{\alpha''}$ into $O3_{\alpha''}$. Thus, the orientation relationship between $O1_{\alpha''}$ and $O3_{\alpha''}$ is a twinning relationship corresponding to a new $\{130\}<310>_{\alpha''}$ compound twinning system which was never reported in α" phase of titanium based alloys. However, this twinning system was reported to be the most common in the α phase of uranium [33] which has the same crystallographic structure than the α" phase in titanium. Moreover, recent calculations concerning nanodomains

occurring in some specific titanium alloys demonstrated that this twinning system is the easiest to form in a tetragonal structure close to the orthorhombic structure of α" [19]. Occurrence of this new twinning system in orthorhombic α" martensite is then in accordance with literature concerning close structures.

Some larger deformation bands in Fig. 4b are divided in two domains with $O3_{\alpha''}$ and $O4_{\alpha''}$ orientation, respectively. In such a case, they share a $<211>_{\alpha''}$ direction (Fig. 5c and 5d) around which a rotation of 180° transforms $O3_{\alpha''}$ into $O4_{\alpha''}$, corresponding to the $<211>_{\alpha''}$ type II twinning system which is observed in selfaccommodating martensite [28,29]. Moreover, no twinning relationship was evidenced between $O1_{\alpha''}$ and $O4_{\alpha''}$, $O2_{\alpha''}$ and $O4_{\alpha''}$, $O2_{\alpha''}$ and $O3_{\alpha''}$. One can however notice that a $\{111\}_{\alpha"}$ pole is nearly common between $O2_{\alpha''}$ and $O4_{\alpha''}$ but a rotation of 180° around it shows that there is no twinning relationship between these two orientations. Consequently to all these observations, it seems that these larger bands are undergoing reorientation. This point will be discussed further in the section 5.3.

4.2. Correspondence with the β phase

In order to better understand the characteristics of the different twins observed in α" martensite, an application of the orientation relationship between α" and β phases can bring some interesting highlights. It has been previously shown that electron backscattered patterns (EBSP) obtained for a microstructure composed of α" (Fig. 4b for example) can be directly indexed by the β phase, even if no β phase is present in the microstructure. This procedure was proved to be a way to apply directly the OR between β and α'' phase and operates as a crystallographic reconstruction of the high temperature β phase [32].

This method was thus applied to the EBSD data of the Fig. 4b to obtain the same EBSD map indexed by the β phase only (Fig. 4c). Only two orientations are measured in the grain studied in the previous section: $O1_{\beta}$ is the orientation of the parent grain and $O2_{\beta}$ is the orientation of the apparent twin. By comparison of Fig. 4b and Fig. 4c, one can conclude that $O1_{\alpha''}$ and $O2_{\alpha''}$ correspond to the same orientation of the β phase $O1_{\beta}$. Similarly, $O3_{\alpha''}$ and $O4_{\alpha''}$, which were detected in larger twins, correspond to a unique orientation of the β phase $O2_{\beta}$. The resultant $\{111\}_{\alpha''}$ and $<211>_{\alpha''}$ twinning systems do not affect the orientation of the high temperature β phase and correspond well to a reorientation process. This result is coherent with the fact that heating such a reoriented microstructure leads to shape memory effect.

As previously, the corresponding stereographic projections of $O1_{\beta}$ and $O2_{\beta}$ were constructed (Fig. 6). The comparison of the orientation of the grain (Fig. 6a) and the twin (Fig. 6b) shows the presence of a common $\{332\}_{\beta}$ plane and a $<113>_{\beta}$ direction around which a rotation of 180° transforms the twin in the parent crystal. This corresponds to the classical $\{332\}<113>_{\beta}$ compound twinning system of metastable β titanium alloys. Consider now the $\{130\}<310>_{\alpha''}$ twinning relationship between the apparent parent grain and the apparent twin, which is found between $O1_{\alpha''}$ and $O3_{\alpha''}$ when EBSPs are indexed by α'' phase (Fig. 5). One can observe on Fig. 5a and Fig. 6a that $(1\bar{3}0)_{\alpha''}$ and $[310]_{\alpha''}$ of $O1_{\alpha''}$ correspond to $(\bar{3}23)_{\beta}$ and $[13\bar{1}]_{\beta}$ of $O1_{\beta}$ respectively, with a misfit lower than 2°, showing a very close correspondence between these two twinning systems. The $\{130\}<310>_{\alpha''}$ twins lead thus to a permanent strain after heating and correspond to plastic deformation. In order to differentiate this twinning system from reorientation ones, it will be named plastic twinning in the rest of this paper.

Table 2 summarizes the twinning systems which are observed when EBSPs are indexed by α'' phase and β phase.

Table 2. Twinning systems observed in strained Ti-25Ta-20Nb alloy.

Phase	Type	K1	η1	K2	η2	Misorientation Rotation axis	
α''	I	(111)				87° - <011>	Reorientation [27-29]
α''	II		[211]			87° - <011>	Reorientation [27-29]
α''	compound	(130)			[110]	53° - <011>	Plastic [present paper]
β	compound	(332)			[111]	50° - <011>	Plastic [26]

4.3. TEM analysis

TEM observations are also performed in order to confirm the previously described EBSD analysis. Similarly, specimens after deformation are observed with a special attention to identification of twins. A typical example of twins is shown in Fig. 7a with the corresponding Selected Area Electron Diffraction (SAED) pattern of both crystals in Fig. 7b. For a better readability, SAED patterns for each crystal are obtained with a smaller aperture and are indexed separately in Fig. 7c for the matrix and Fig. 7d for the twin. The $[001]_{\alpha''}$ zone axis of the matrix is thus parallel to the $[51\bar{2}]_{\alpha''}$ zone axis of the twin that does not corresponds to any known twinning orientation relationship. Especially, this orientation relationship does not correspond to a $\{130\}<310>_{\alpha''}$ twin because the $[001]_{\alpha''}$ axis of the matrix has to be parallel to the $[001]_{\alpha''}$ axis of the twin for this twinning system. However, after a rotation of 180° around the $[\bar{2}11]_{\alpha''}$ direction of the twin, the new position of the $(130)_{\alpha''}$ pole visible on Fig. 7d is the same than a $\{130\}_{\alpha''}$ pole of the matrix. This new orientation of the twin is then in

{130}<310>$_{\alpha''}$ twinning relationship with the matrix. TEM observations confirm thus on one hand that {130}<310>$_{\alpha''}$ twins occur during plastic deformation of α" martensite and, on the other hand, that these twins are afterward reorientated with a <211>$_{\alpha''}$ type II twinning system when the deformation increases.

5. Prediction of activated twinning systems

As shown in Table 2, twinning elements of plastic twinning systems are known while only the twinning plane or the twinning direction are known for reorientation twinning systems. This is why maximum Schmid factor analysis can be used for plastic twinning in order to try to predict activation of different twins during deformation whereas only lattice deformation of CV can be used for reorientation twins.

5.1. Maximum lattice deformation of CV

Once the lattice parameters of α'' phase and β phase are determined, it is possible to calculate the principal strains during the β to α'' transformation:

Where $a_{\alpha''}$, $b_{\alpha''}$ and $c_{\alpha''}$ are the lattice parameters of α'' phase and a_{β} is the lattice parameter of β phase. The lattice deformation that is generated by the formation of each CV can be then calculated from lattice deformation matrices given in [27]. As an example, the lattice deformation matrix of CV1 is:

The tensile direction ***T*** is then marked as a columnar vector in the coordinate system of β phase crystal. Strain along the tensile direction given by the transformation of a β grain into the *i*th CV is finally:

$\varepsilon_i = T^t \varepsilon^{(i)} T$

Then, it is possible to determine which CV maximizes the strain along the tensile direction for each β grain orientation.

The observed CVs are determined by comparing the α'' and β orientations and according to the conventions listed in Table 1. The tensile direction ***T*** is measured from stereographic projections of β crystals (Fig. 6 for example). For the main grain of Fig. 4, the predominant orientation of martensite $O1_{\alpha''}$ corresponds thus to CV4 and leads to a strain of 4.4% along the tensile direction, which is the maximum strain among the 6 CVs. This grain is a particular case, since it is not fully reoriented but analysis of around 50 grains showed that the reorientation is generally finished at this stage of deformation (see for example other grains in Fig. 4) and the observed variant is always the one which corresponds to the maximum lattice deformation along the tensile direction. The reorientation process is then confirmed to operate as a selection of CV promoting the one leading to a maximum of strain.

5.2 Schmid Factor analysis

When α" grains are reorientated, the activation of plastic twinning can be investigated by a Schmid Factor (SF) analysis. The SF is defined similarly to slip as:

$SF = \cos\lambda \cos\phi$

where λ is the angle between the tensile direction and the normal of the twinning plane K_1 and ϕ is the angle between the tensile direction and the twinning direction η_1. The values of λ and ϕ are taken between 0° and 180° in order to obtain SF values between -0.5 and 0.5. Using this convention, a variant whose SF is positive leads to an elongation along the tensile direction and will accommodate a tensile stress. SF analysis was successfully used to predict the activation of twinning systems [26,34,35] including {332}<113> in metastable β titanium alloys [18,36]. However, signs of normal to K_1 and η_1 must be chosen carefully. Indeed, an important difference between twinning and slip of perfect dislocations is the polarity of twinning. This means that the slip of a partial dislocation in the opposite sense of the twinning direction (antitwinning direction) would not produce a twin since energetically unfavorable [26]. As a consequence, activated variants under a uniaxial tensile stress will be different from those activated under a uniaxial compression stress in the same direction. In order to apply the Schmid law and distinguish the variants that can be activated during a tensile test, the sign of the indices of each variant must be defined in accordance with the usual criterions [26] in order to distinguish the variants leading to elongation or compression along the applied stress direction. Due to the lower symmetry of α" martensite, only two variants of $\{130\}\langle 310\rangle_{\alpha''}$ twins can be formed while there are twelve variants of $\{332\}\langle 113\rangle_{\beta}$ twins in the β phase. The exact twinning elements of each variant used in the present SF analysis are given in Table 3 and the method to establish them is described in Appendix A.

Table 3. Twinning elements of each variant used for Schmid Factor analysis for $\{130\}\langle 310\rangle_{\alpha''}$ and $\{332\}\langle 113\rangle_{\beta}$ twinning systems.

Variant	K_1	η_1	K_2	η_2
$V1_{\alpha''}$ $V2_{\alpha''}$				
$V1_{\beta}$ $V2_{\beta}$ $V3_{\beta}$ $V4_{\beta}$				

$V5_{\beta}$				
$V6_{\beta}$				
$V7_{\beta}$				
$V8_{\beta}$				
$V9_{\beta}$				
$V10_{\beta}$				
$V11_{\beta}$				
$V12_{\beta}$				

Schmid factor calculation is first used to analyze the activation of the {130}<310>$_{\alpha''}$, i.e. between $O1_{\alpha''}$ and $O3_{\alpha''}$ in Fig. 4. The tensile direction in the coordinate system of $O1_{\alpha''}$ is [$\bar{6}$ and then SF are calculated for the two variants. SF of $V1_{\alpha''}$ is 0.20 while SF of $V2_{\alpha''}$, which is actually activated, is 0.43 which is quite close to the maximum value. The activated variant is thus the one with the highest SF and selection of variants for {130}<310>$_{\alpha''}$ twinning in α" martensite obeys the Schmid law.

As there is a correspondence between {130}<310>$_{\alpha''}$ in α" phase and {332}<113>$_{\beta}$ in β phase, the same calculus is made for each variant of the {332}<113>$_{\beta}$ system corresponding to the grain previously analyzed in Fig. 4. As the K_1 and η_1 of $V8_{\beta}$ correspond to K_1 and η_1 of $V2_{\alpha''}$, the SF of $V8_{\beta}$ is also 0.43. This value is also the highest SF among the 12 variants of {332}<113>$_{\beta}$ twinning system. Schmid Factor analysis has been performed on more than 10 plastic twins and predicts correctly the variant which is activated in β phase as well as in α" phase. This point will be discussed more precisely in section 6.

5.3 Sequence of deformation

Analysis of lattice deformation and SF shows that the deformation is first accommodated by reorientation of selfaccommodating martensite via {111}$_{\alpha''}$ or <211>$_{\alpha''}$ twinning systems. At the end of this step, the α" variant which gives the maximum of strain along the tensile direction occupies the whole ex-β grain. Next, {130}<310>$_{\alpha''}$ twins ensure the plastic

deformation of this unique variant such as the transformation of $O1_{\alpha''}$ into $O3_{\alpha''}$ in Fig. 4 for example. However, this new crystallographic orientation of the twin may be not the CV which leads to the maximum lattice deformation along the tensile direction since this deformation mechanism is not reorientation. New lattice deformations are thus calculated for $O3_{\alpha''}$ using the corresponding orientation of β phase $O2_{\beta}$ since the β crystal has been reoriented by plastic twinning. $O3_{\alpha''}$ corresponds thus to CV3 and leads to a deformation of -1.90% regarding the β to α" transformation, which means that this CV is not favorable when a tensile stress is applied and can be reoriented. On Fig. 4b, $O3_{\alpha''}$ is observed to be reoriented into $O4_{\alpha''}$ using a $<211>_{\alpha''}$ type II reorientation twinning and $O4_{\alpha''}$ corresponds to CV6. Among the 6 possible CVs, this CV6 has the maximum strain along the tensile direction (4,91%). It appears that, when plastic twins are formed, their crystallographic orientation does not correspond to the most favorable CV and a reorientation process takes place once again in order to transform the twin into the most favorable CV regarding the orientation of the applied stress. Such reorientation process of plastic twins was never reported in α" titanium based alloys and shows the occurrence of a continuous reorientation of the new plastic twins formed during the deformation.

To summarize, the following sequence of deformation mechanisms during the tensile test are deduced from the former observations and analysis:

- selfaccommodating microstructure is first reoriented using $\{111\}_{\alpha''}$ and $<211>_{\alpha''}$ twinning systems – the CV which leads to the maximum lattice deformation is selected;
- plastic $\{130\}<310>_{\alpha''}$ twinning occurs next, leading to permanent strain – the variant selection of this twinning system follows the Schmid law;

- plastic twins are finally reoriented using the same reorientation twinning systems than in the early stage of deformation – this step increases the recoverable strain by shape memory effect after heating even if plastic deformation has occurred.

6. Comparison of Schmid Factor analysis in α'' and β phases

It was shown in section 5.2 that Schmid factor analysis is as relevant when EBSPs are indexed by α'' phase than when they are indexed by β phase, i.e. predicting of activated twins in α" is equivalent to predicting the corresponding twins in the high temperature β phase. This is due to the fact that each twinning element (K_1, K_2, $\eta_1\eta_{,2}$) of a {130}<310>$_{\alpha"}$ variant coincides with each twinning element of a {332}<113>$_{\beta}$ variant. As twinning elements coincide exactly, the value of SF is necessary the same. However, the reciprocity of this statement is not true since {332}<113>$_{\beta}$ system has twelve twinning variants while {130}<310>$_{\alpha"}$ has only two ones. Consequently, only two {332}<113>$_{\beta}$ variants correspond to {130}<310>$_{\alpha"}$ twins for one given α" CV. The reason why the activated {130}<310>$_{\alpha"}$ twin always corresponds to the {332}<113>$_{\beta}$ with the highest SF in the β phase is clarified hereafter.

For each CV of α", twinning elements of {130}<310>$_{\alpha"}$ twin variants coincide with twinning elements of different {332}<113>$_{\beta}$ twin variants in the β phase. Table 4 summarizes these correspondences as a function of the activated α" CV and according to the notations given in Table 3. As an example, the twin variant $V1_{\beta}$ of {332}<113>$_{\beta}$ corresponds to the twin variant $V2_{\alpha''}$ of {130}<310>$_{\alpha"}$ when the CV5 of α" is formed. This means that the activation of a {130}<310>$_{\alpha''}$ twin which would correspond to the activation of $V1_{\beta}$ is only possible if the grain has been reoriented into CV5.

Table 4. Correspondence between {332}<113>$_{\beta}$ variants and {130}<310>$_{\alpha"}$ twinning system depending on the activated α" CV.

{332}<113>$_{\beta}$ variant	CV and {130}<310>$_{\alpha''}$ variant
$V1_{\beta}$	$CV5 – V2_{\alpha''}$
$V2_{\beta}$	$CV3 – V2_{\alpha''}$
$V3_{\beta}$	$CV1 – V1_{\alpha''}$
$V4_{\beta}$	$CV6 – V1_{\alpha''}$
$V5_{\beta}$	$CV3 – V1_{\alpha''}$
$V6_{\beta}$	$CV2 – V2_{\alpha''}$
$V7_{\beta}$	$CV6 – V2_{\alpha''}$
$V8_{\beta}$	$CV4 – V1_{\alpha''}$
$V9_{\beta}$	$CV1 – V2_{\alpha''}$
$V10_{\beta}$	$CV5 – V1_{\alpha''}$
$V11_{\beta}$	$CV4 – V2_{\alpha''}$
$V12_{\beta}$	$CV2 – V1_{\alpha''}$

Fig. 8 corresponds to graphical representation of the data given in Table 4. Fig. 8a is an inverse pole figure (IPF) which covers the full orientation domain of a β crystal and indicates the domains of maximum lattice deformation along the tensile direction, each domain corresponding to a given α" CV. Fig. 8b similarly indicates the domains of highest SF (SF>0.4) of {332}<113>$_{\beta}$ variants, again as a function of the tensile direction. Using Fig. 8 and Table 4, one can see that the orientation domain for the activation of each variant of {332}<113>$_{\beta}$ coincides with the orientation domain of one α" CV. By taking the example of the grain studied previously, we found in the section 5.2 that the twin in the corresponding high temperature β phase is the variant $V8_{\beta}$ and the parent grain in the observed α" microstructure has a $O1_{\alpha"}$ orientation corresponding to the CV4. The orientation domain of $V8_{\beta}$ effectively coincides with the orientation domain of CV4 in Fig. 8. This proves that, from a selfaccommodating α" microstructure, the prediction of activated {130}<310>$_{\alpha"}$ plastic twins by using a combination of maximum lattice deformation and α'' Schmid factor analysis is equivalent to simply use a Schmid factor analysis to predict the {332}<113>$_{\beta}$ which would be activated in the β phase, even if the phase is not present.

Conclusion

Mechanisms of deformation of the shape memory α" Ti-25Ta-20Nb alloy were studied. When an external stress is applied, the selfaccommodating α" microstructure is shown to be reoriented by $\{111\}_{\alpha''}$ type I and $<211>_{\alpha''}$ Type II reorientation twinning systems. EBSD measurements confirm that these twinning systems do not modify the corresponding β phase orientation. This alloy also undergoes a new $\{130\}<310>_{\alpha''}$ plastic twinning system which was never reported before.

A complex three-step sequence of deformation was revealed, consisting of the successive activation of:

- reorientation twinning so as to obtain one unique α" CV per ex-β grain
- plastic twinning
- reorientation of the plastic twin

It was shown that maximum lattice deformation is a relevant parameter to predict the reoriented CV and Schmid factor analysis can be used to predict plastic twinning.

A strong correspondence between $\{130\}<310>_{\alpha''}$ and $\{332\}<113>_{\beta}$ is observed: twinning elements of α'' twinning system correspond to β twinning system ones. Moreover, the CV selection during reorientation tends to make α'' twinning coincide with variants of β twinning whose SF is the highest. Thus, Schmid factor analysis in the β phase is equivalent to the combination of maximum lattice deformation and Schmid factor analysis in α".

Acknowledgement

The authors acknowledge the THEMIS platform of the University of Rennes for providing access to TEM facilities.

Appendix A: Determination of the sign of twinning elements of each variant of a twinning system

According to Christian and Mahajan [26], the original (parent) lattice is reoriented by atom displacements which are equivalent to a simple shear of the lattice points, or of some integral fraction of these points in the classical theory of deformation twinning. The invariant plane of this shear is called (K_1) and the shear direction η_1; the second undistorted (or conjugate) plane is (K_2), the plane containing η_1 and the normal directions to (K_1) and (K_2) is the plane of shear, here denoted by (P), and the intersection of (K_2) and (P) is the conjugate shear direction η_2. These elements are schematized in Fig A.1. Conventionally, the normal directions to (K_1) and (K_2), noted $\mathbf{K_1}$ and $\mathbf{K_2}$ respectively, are chosen so that the normal to (K_1) is facing up and the normal to (K_2) is facing right in Figure A.1.

Given this convention, twinning elements must follow the following rules:

- $\mathbf{K_1}.\eta_1=0$ where $\mathbf{K_1}$ is the pole of (K_1): η_1 is included in (K_1)
- $\mathbf{K_2}.\eta_2=0$ where $\mathbf{K_2}$ is the pole of (K_2): η_2 is included in (K_2)
- $\eta_1.\eta_2<0$ obtuse angle between η_1 and η_2 is necessary to twinning
- $\mathbf{K_1}.\mathbf{K_2}>0$ this condition comes from the convention for $\mathbf{K_1}$ and $\mathbf{K_2}$

Signs of $\mathbf{K_1}$, $\mathbf{K_2}$, η_1 and η_2 of each variant of a twinning system are thus chosen in order to follow these rules.

References

[1] Y.L. Hao, S.J. Li, S.Y. Sun, C.Y. Zheng, R. Yang, Elastic deformation behaviour of Ti-24Nb-4Zr-7.9Sn for biomedical applications, Acta Biomater. 3 (2007) 277-286.

[2] M. Tahara, H.Y. Kim, H. Hosoda, S. Miyazaki, Cyclic deformation behavior of a Ti-26 at.% Nb alloy, Acta Mater. 57 (2009) 2461-2469.

[3] F. Sun, Y.L. Hao, S. Nowak, T. Gloriant, P. Laheurte, F. Prima, A thermo-mechanical treatment to improve the superelastic performances of biomedical Ti–26Nb and Ti–20Nb–6Zr (at.%) alloys, J. Mech. Behav. Biomed. Mater. 4 (2011) 1864-1872.

[4] M. Tahara, H.Y. Kim, T. Inamura, H. Hosoda, S. Miyazaki, Lattice modulation and superelasticity in oxygen-added β-Ti alloys, Acta Mater. 59 (2011) 6208-6218.

[5] A. Ramarolahy, P. Castany, F. Prima, P. Laheurte, I. Péron, T. Gloriant, Microstructure and mechanical behavior of superelastic Ti-24Nb-0.5O and Ti-24Nb-0.5N biomedical alloys, J. Mech. Behav. Biomed. Mater. 9 (2012) 83-90.

[6] Y.L. Hao, Z.B. Zhang, S.J. Li, R. Yang, Microstructure and mechanical behavior of a Ti–24Nb–4Zr–8Sn alloy processed by warm swaging and warm rolling, Acta Mater. 60 (2012) 2169-2177.

[7] M. Abdel-Hady Gepreel, M. Niinomi, Biocompatibility of Ti-alloys for long-term implantation, J. Mech. Behav. Biomed. Mater. 20 (2013) 407-415.

[8] M.F. Ijaz, H.Y. Kim, H. Hosoda, S. Miyazaki, Effect of Sn addition on stress hysteresis and superelastic properties of a Ti–15Nb–3Mo alloy, Scripta Mater. 72–73 (2014) 29-32.

[9] Y. Yang, P. Castany, M. Cornen, I. Thibon, F. Prima, T. Gloriant, Texture investigation of the superelastic Ti–24Nb–4Zr–8Sn alloy, J. Alloys Compd. 591 (2014) 85-90.

[10] M.F. Ijaz, H.Y. Kim, H. Hosoda, S. Miyazaki, Superelastic properties of biomedical (Ti–Zr)–Mo–Sn alloys, Mater. Sci. Eng. C 48 (2015) 11-20.

[11] H.Y. Kim, Y. Ikehara, J.I. Kim, H. Hosoda, S. Miyazaki, Martensitic transformation, shape memory effect and superelasticity of Ti-Nb binary alloys, Acta Mater. 54 (2006) 2419-2429.

[12] E.G. Obbard, Y.L. Hao, T. Akahori, R.J. Talling, M. Niinomi, D. Dye, R. Yang, Mechanics of superelasticity in Ti–30Nb–(8–10)Ta–5Zr alloy, Acta Mater. 58 (2010) 3557-3567.

[13] E. Bertrand, P. Castany, T. Gloriant, Investigation of the martensitic transformation and the damping behavior of a superelastic Ti–Ta–Nb alloy, Acta Mater. 61 (2013) 511-518.

[14] P. Castany, A. Ramarolahy, F. Prima, P. Laheurte, C. Curfs, T. Gloriant, In situ synchrotron X-ray diffraction study of the martensitic transformation in superelastic Ti-24Nb-0.5N and Ti-24Nb-0.5O alloys, Acta Mater. 88 (2015) 102-111.

[15] Y. Yang, P. Castany, M. Cornen, F. Prima, S.J. Li, Y.L. Hao, T. Gloriant, Characterization of the martensitic transformation in the superelastic Ti–24Nb–4Zr–8Sn alloy by in situ synchrotron X-ray diffraction and dynamic mechanical analysis, Acta Mater. 88 (2015) 25-33.

[16] S. Sadeghpour, S.M. Abbasi, M. Morakabati, Deformation-induced martensitic transformation in a new metastable β titanium alloy, J. Alloys Compd. 650 (2015) 22-29.

[17] S. Hanada, O. Izumi, Transmission electron microscopic observations of mechanical twinning in metastable beta titanium alloys, Metall. Trans. A 17 (1986) 1409-1420.

[18] E. Bertrand, P. Castany, I. Péron, T. Gloriant, Twinning system selection in a metastable β-titanium alloy by Schmid factor analysis, Scripta Mater. 64 (2011) 1110-1113.

[19] H. Tobe, H.Y. Kim, T. Inamura, H. Hosoda, S. Miyazaki, Origin of {332} twinning in metastable β-Ti alloys, Acta Mater. 64 (2014) 345-355.

[20] H. Zhan, W. Zeng, G. Wang, D. Kent, M. Dargusch, On the deformation mechanisms and strain rate sensitivity of a metastable β Ti–Nb alloy, Scripta Mater. 107 (2015) 34-37.

[21] M. Besse, P. Castany, T. Gloriant, Mechanisms of deformation in gum metal TNTZ-O and TNTZ titanium alloys: A comparative study on the oxygen influence, Acta Mater. 59 (2011) 5982-5988.

[22] P. Castany, M. Besse, T. Gloriant, Dislocation mobility in gum metal beta-titanium alloy studied via in situ transmission electron microscopy, Phys. Rev. B 84 (2011) 020201.

[23] P. Castany, M. Besse, T. Gloriant, In situ TEM study of dislocation slip in a metastable β titanium alloy, Scripta Mater. 66 (2012) 371-373.

[24] E. Farghadany, A. Zarei-Hanzaki, H.R. Abedi, D. Dietrich, M.R. Yadegari, T. Lampke, The coupled temperature–strain rate sensitivity of Ti–29Nb–13Ta–4.6Zr alloy, Mater. Sci. Eng. A 610 (2014) 258-262.

[25] J.P. Morniroli, M. Gantois, Etude des conditions de formation de la phase omega dans les alliages titane-niobium et titane-molybdène, Mem. Sci. Rev. Metal. 11 (1973) 831-842.

[26] J.W. Christian, S. Mahajan, Deformation twinning, Prog. Mater. Sci. 39 (1995) 1-157.

[27] T. Inamura, J.I. Kim, H.Y. Kim, H. Hosoda, K. Wakashima, S. Miyazaki, Composition dependent crystallography of α"-martensite in Ti-Nb-based β-titanium alloy, Philos. Mag. 87 (2007) 3325-3350.

[28] Y.W. Chai, H.Y. Kim, H. Hosoda, S. Miyazaki, Self-accommodation in Ti-Nb shape memory alloys, Acta Mater. 57 (2009) 4054-4064.

[29] H. Tobe, H.Y. Kim, T. Inamura, H. Hosoda, T.H. Nam, S. Miyazaki, Effect of Nb content on deformation behavior and shape memory properties of Ti–Nb alloys, J. Alloys Compd. 577S (2013) S435-S438.

[30] K. Otsuka, X. Ren, Physical metallurgy of Ti-Ni-based shape memory alloys, Prog. Mater. Sci. 50 (2005) 511-678.

[31] D.H. Ping, Y. Yamabe-Mitarai, C.Y. Cui, F.X. Yin, M.A. Choudhry, Stress-induced alpha" martensitic (110) twinning in beta -Ti alloys, Appl. Phys. Lett. 93 (2008) 151911-151913.

[32] E. Bertrand, P. Castany, T. Gloriant, An alternative way to orient the parent phase in the cubic/orthorhombic martensitic transformation of titanium shape memory alloys, Scripta Mater. 83 (2014) 41-44.

[33] R.W. Cahn, Plastic deformation of alpha-uranium; twinning and slip, Acta Metall. 1 (1953) 49-70.

[34] T. Sawai, A. Hishinuma, Twin intersection in tensile deformed γ-TiAl intermetallic compounds, J. Phys. Chem. Solids 66 (2005) 335-338.

[35] S. Godet, L. Jiang, A.A. Luo, J.J. Jonas, Use of Schmid factors to select extension twin variants in extruded magnesium alloy tubes, Scripta Mater. 55 (2006) 1055-1058.

[36] X.H. Min, K. Tsuzaki, S. Emura, T. Sawaguchi, S. Ii, K. Tsuchiya, {332}<113> Twinning system selection in a β-type Ti–15Mo–5Zr polycrystalline alloy, Mater. Sci. Eng. A 579 (2013) 164-169.

Figure 1

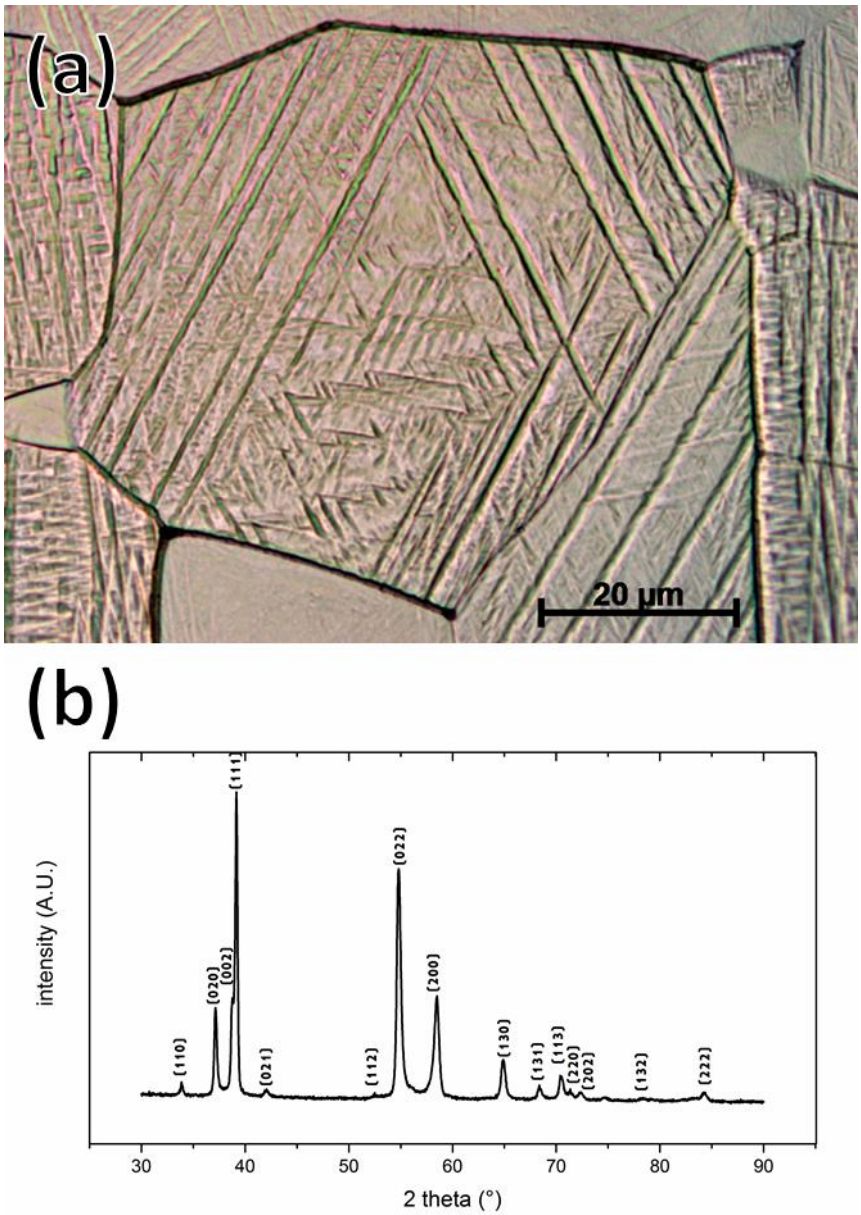

Fig. 1. Optical micrograph of recrystallized Ti-25Ta-20Nb alloy (a) and X-rays diffractogram (b)

Figure 2

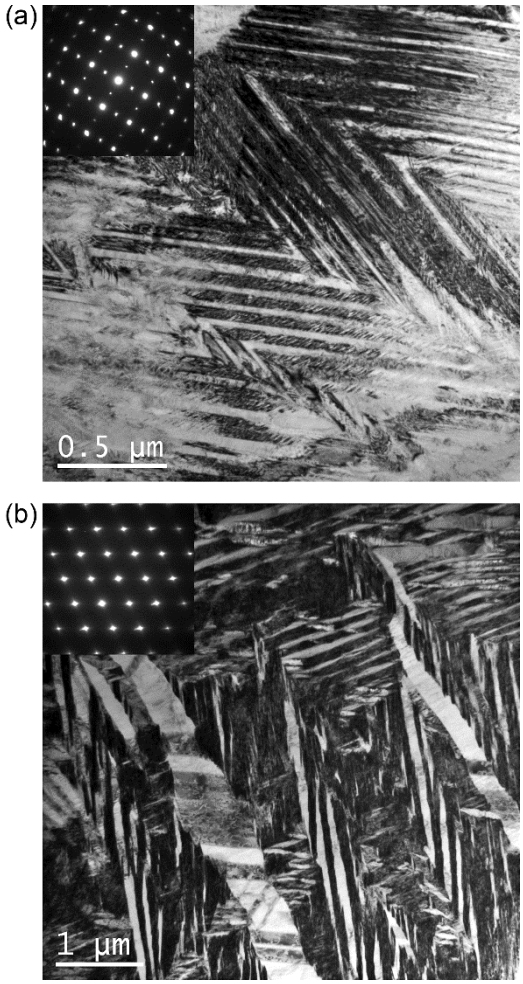

Fig. 2. Bright field TEM micrographs of the initial microstructure with (a) typical V-shaped martensite morphology or (b) more complex arrangement of martensite plates.

Figure 3

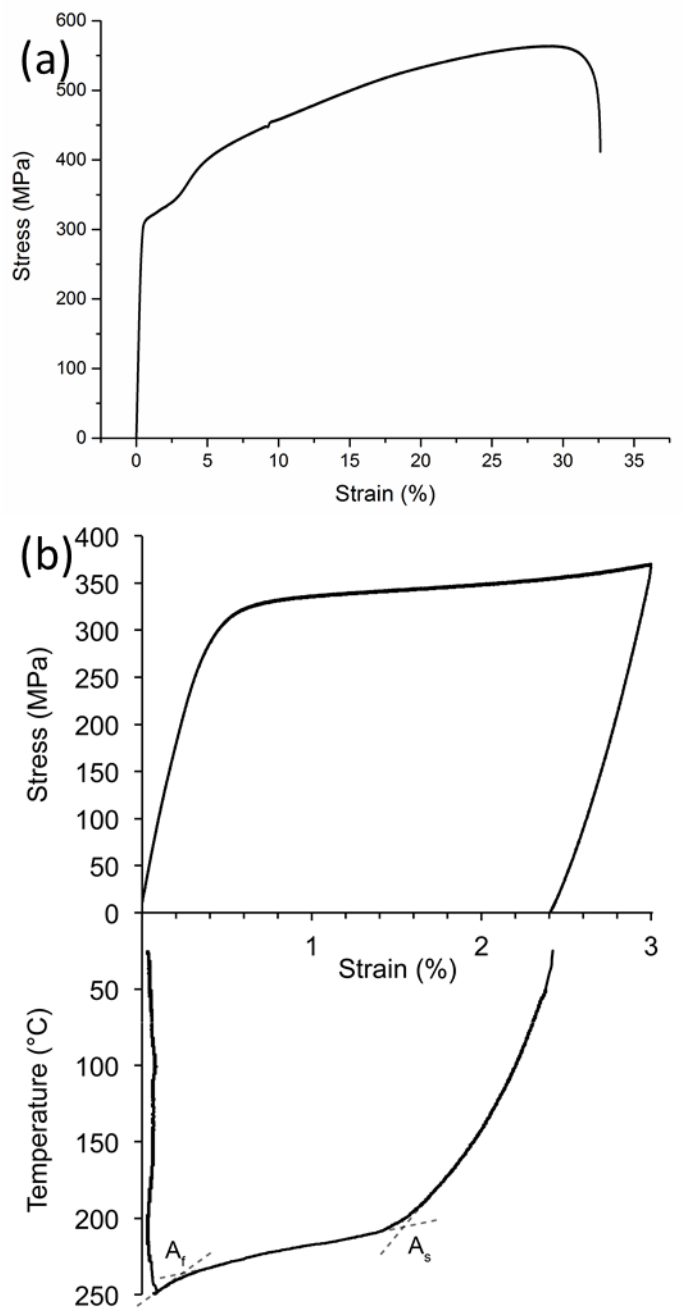

Fig. 3. Tensile test of Ti-25Ta-20Nb (a) and interrupted tensile test after 3% strain followed by heating from 20 °C to 250 °C.

Figure 4

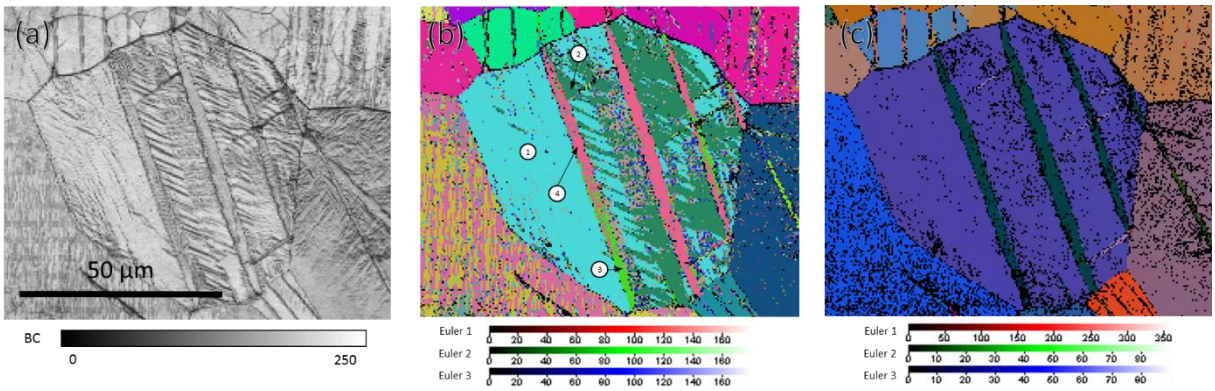

Fig. 4. EBSD maps of Ti–25Ta–20Nb alloy strained until 6%: (a) band contrast (BC) only, (b) Euler angles obtained from indexation with the α'' phase and (c) Euler angles obtained from indexation with the β phase.

Figure 5

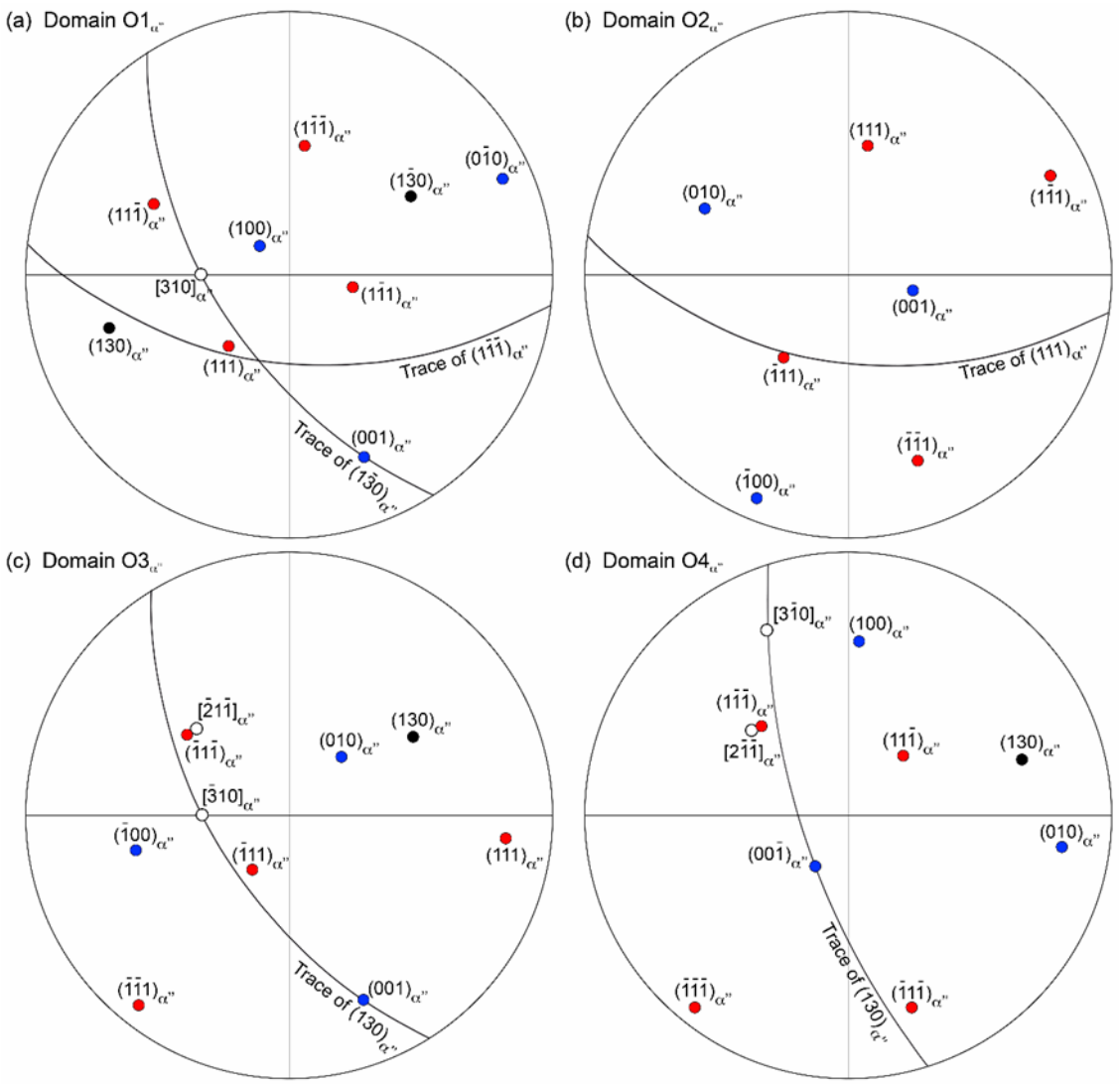

Fig. 5. Stereographic projections of all α'' orientations observed in the ex-β grain of Fig. 4b.

Figure 6

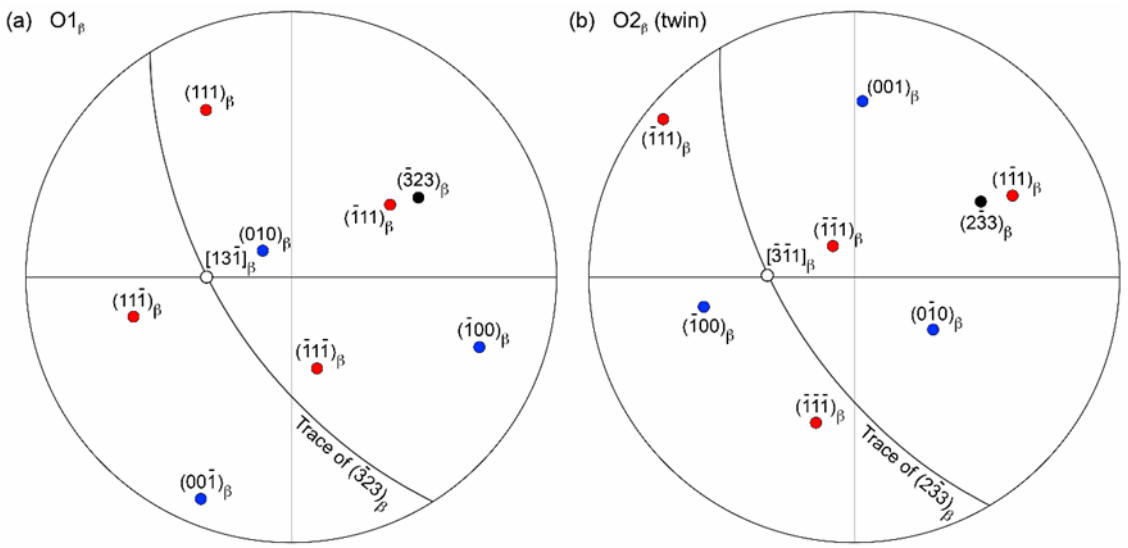

Fig. 6. Stereographic projections of β orientations obtained from the grain of Fig. 4c.

Figure 7

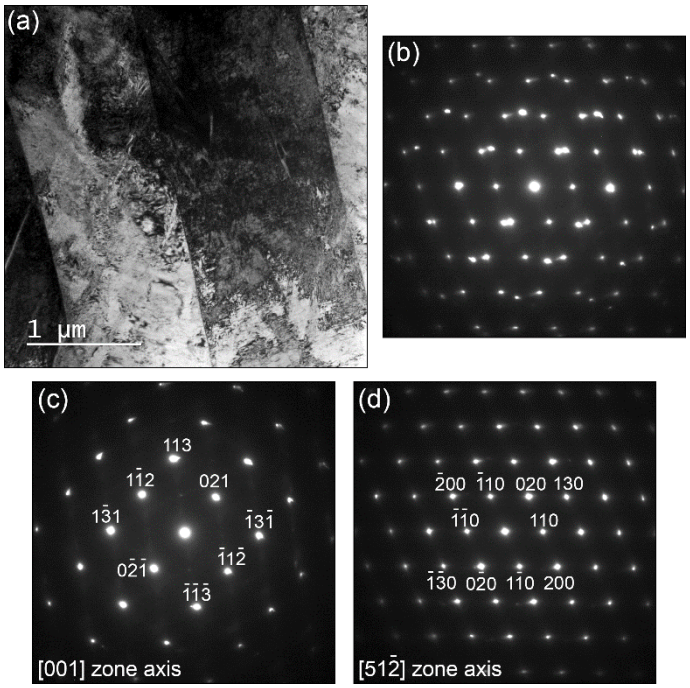

Fig. 7. Bright field image of plastic twins in a strained α'' microstructure (a) and the corresponding common diffraction patterns of both matrix and twins (b); diffraction patterns of matrix only (c) and twin only (d) are indexed separately.

Figure 8

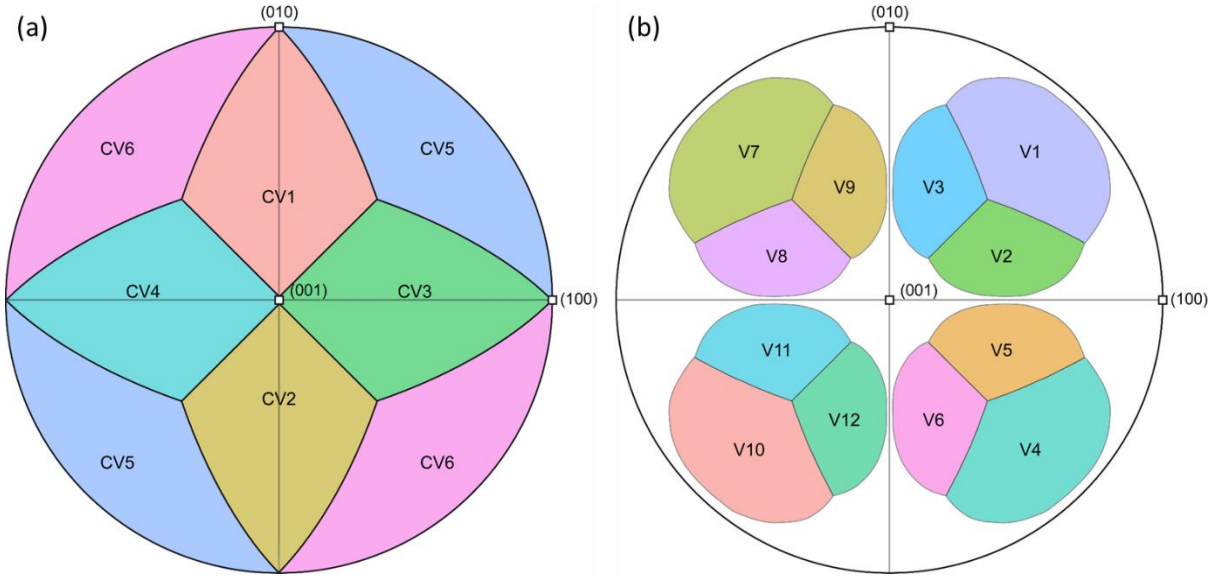

Fig. 8. Inverse pole figure (IPF) indicating the maximum transformation strain domains for each activated α'' CV (a) and the domains with SF>0.4 for each {332}<113>$_\beta$ variant (b) as a function of the orientation of the tensile direction in a β crystal.

Figure A1

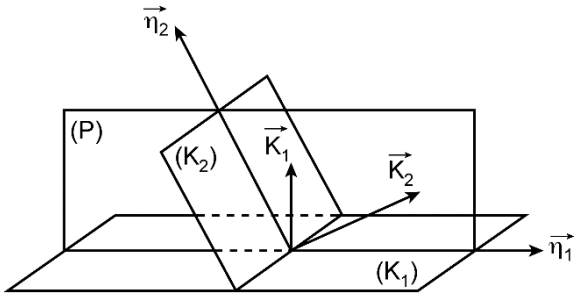

Fig A.1. The four twinning elements. The twinning and the conjugate (or reciprocal) twinning planes are (K_1) and (K_2) and the twinning and conjugate (or reciprocal) twinning directions are η_1 and η_2, respectively. The four twinning elements are contained in the plane of shear (P).

Graphical Abstract